Construction of specific nickel-based electrode using N,N-dimethylformamide/water as solvent and the application in metronidazole detection

Yunfan Lu[a], Ruibin Wang[a],*, Guoping Wang[a],*, Nian Chen[b],*

[a]School of Chemistry and Chemical Engineering, University of South China, Hengyang 421001, China, emails: rbwang@usc.edu.cn (R. Wang), 2005000784@usc.edu.cn (G. Wang), 3448713229@qq.com (Y. Lu)
[b]The First Affiliated Hospital, Department of Medical Cosmetic, Hengyang Medical School, University of South China, Hengyang 421001, China, email: chenniangood@126.com (N. Chen)

ABSTRACT

To achieve rapid detection for metronidazole (MNZ), a mesoporous nickel-based metal–organic framework (Ni-MOF), which had sub-micron-assemblies of layered flakes and abundant carboxyl groups, was synthesized in a particular solvent containing water with a facile one-step hydrothermal method. Using Ni-MOF/multi-walled carbon nanotubes as the sensor electrode, cyclic voltammetry and differential pulse voltammetry were investigated in MNZ solution (containing 0.1 M PBS). The current response linearly varied with MNZ's concentration in the range of 5–100 μM. A relatively low detection limit of 25 nM was obtained, which outperformed many electrochemical platforms for MNZ reported in literatures. Moreover, further investigations indicated this system was endowed with good anti-interference ability repeatability, and long-term stability. The present work was promising to pave the way for the quantitation of MNZ in biomedical and healthcare applications.

Keywords: Metal–organic framework; Metronidazole; Electrochemical sensor; Residue detection

1. Introduction

Metronidazole (MNZ), as a nitroimidazole derivative, has often been used in the clinical treatment of disease-causing bacterial and anaerobic protozoan infections because of its low price and strong bactericidal effect. It is also utilized as a promoter to improve feed efficiency for inducing the growth of cattle, pigs and poultry [1]. However, its side effects are relatively large, and its residues are very harmful to the ecological environment. Many countries and regions have limited the use of MNZ [2] due to its perceived genotoxic, carcinogenic, and mutagenic side effects [3,4]. Thus, its real-time monitoring and determination become very urgent. Several methods have been reported for the determination of MNZ, including immunoassay [5], high-performance liquid chromatography [6–8], thin layer chromatography [9] and spectrophotometry [10–12].

Nevertheless, most of these methods lack simplicity, cost-effectiveness, and accessibility. Electrochemical methods have been widely used in analytical chemistry due to the advantages of simple preparation, fast response, low cost, high sensitivity, and the feasibility of miniaturization [13]. The selectivity of electrochemical sensors mainly depends on the development of chemically modified electrodes [14]. For example, Arturo has prepared an electrochemical sensor for MNZ's determination by modifying carbon paste electrode through the electropolymerization of α-cyclodextrin [15]. Under the optimal condition, the detection limit is 0.28 ± 0.02 μM, and a good linear relationship between the peak current and MNZ concentration is obtained in the MNZ concentration range of 0.5–103.0 mM. Sadeghi et al. developed a screen-printed carbon electrode modified with 1-octyl-3-methylimidazolium hexafluorophosphate and Ag nanoparticles, which shows a detection limit of 0.4 mM and

* Corresponding authors.

a bimodal linear performance when MTZ's concentration ranges within 3.1–310 mM and 310–1,300 mM. Other modified sensors such as Pt nanospheres/polyfurfural film [17], graphene-ionic liquid [18], imprinted polymer [19], and ZIF-67C@rGO [20] have also been developed for MNZ's determination. However, they suffer from either high cost, complicated preparation process, lower sensitivity or poor stability. Metal–organic frameworks (MOFs) are composed of metal ions and organic ligands. They possess tunable pore size, superior porous structure and large specific surface area. In MOFs, the functional groups containing oxygen are beneficial for absorbing and enriching the target molecules, and the metal center can serve as a catalysis center to promote the electrochemical reaction. As the result, the electrochemical signal can be significantly amplified, improving the testing sensitivity and accuracy. Hence, MOFs can be considered as new electrochemical sensors. For example, Wang et al. [21] has utilized Ni(II)-MOF s as an electrode sensor material for the determination of non-enzymatic H_2O_2, which exhibits a detection limit as low as 2.1 μM and a response within 2.5 s.

The reaction conditions, especially, the solvents used, significantly influence the formation of MOFs [22]. Solvents can determine the self-assembly of metals with organic ligands and be expected to change the interfacial free energy of the reaction system [23]. Therefore, using different solvents might give rise to different morphology, particle size, microstructure, specific surface area and electrochemical properties. This stimulated us to synthesize a higher efficient MOFs sensor material by using an appropriate solvent. Here,

nickel-based MOFs were synthesized in different solvents by a one-step hydrothermal method. The solvents involved N,N-dimethylformamide (DMF) and water/DMF. In this work, Ni-MOF was prepared from a mixed solution of DMF and water with a ratio of 5:1 for further study because of its rich mesoporous structure and excellent electrochemical performance.

Under the optimal condition, the as-fabricated Ni-MOFs were endowed with sub-micron assemblies of layered flakes and abundant carboxyl groups. By further combining multi-walled carbon nanotubes with Ni-MOFs, a good linear relationship between the current response and MNZ concentration and a relatively low detection limit of 25 nM was obtained. Besides, good anti-interference ability, repeatability and long-term stability were also observed. These characteristics made Ni-MOFs an outstanding electrochemical platform for highly sensitive MNZ detection in diverse applications.

2. Results and discussion

2.1. Synthesis and characterization of Ni-MOFs

As shown in Fig. 1A and B, the samples showed obvious differences in morphology and particle size. Ni-MOF-1 had many sub-micron-assemblies of layered flake, while Ni-MOF-2 tended to closely agglomerate to form large blocks and almost no pores existed. The water molecules changed the interfacial free energy and accelerated the growth of
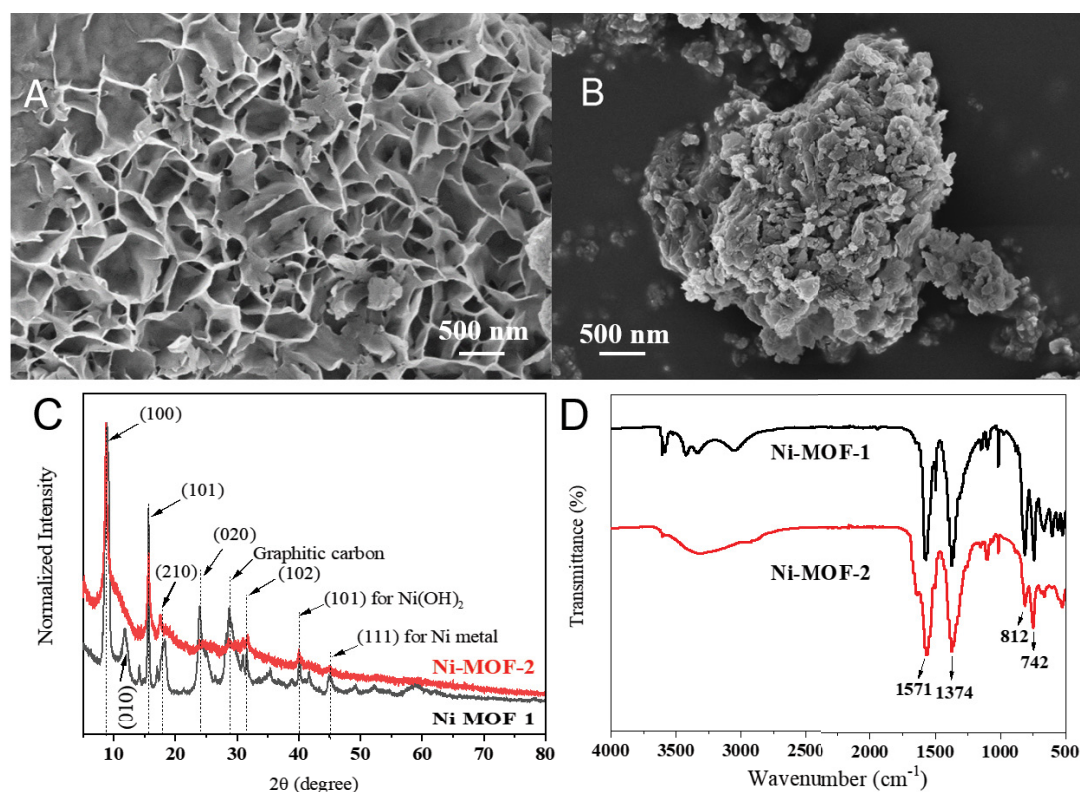

Fig. 1. Scanning electron microscopy images of (A) Ni-MOF-1, (B) Ni-MOF-2, (C) X-ray diffraction patterns and (D) Fourier-transform infrared spectra of Ni-MOF-1 and Ni-MOF-2.

crystals in specific directions [24], resulting in different morphology and crystallinity. The X-ray diffraction (XRD) patterns of MOFs are shown in Fig. 1C. The diffraction pattern of Ni-MOF-1 was in good agreement with the MOFs synthesized by Ni ions and terephthalic acid ligands from other reports [22,25], The diffraction peaks appearing around 9, 12, 15, 18, 24, 28, 32, 40, and 45 were corresponded to (100), (010), (101), (210), (020), graphitic carbon, (102), (101) for Ni(OH)$_2$ and (111) for Ni metal facet, respectively (simulated from single-crystal [Ni$_3$(OH)$_2$(C$_8$H$_4$O$_4$)$_2$(H$_2$O)$_4$]·2H$_2$O, CCDC no. 638866, [25,26]). Apparently, all reflection planes were observed in both samples, except the (010) peak is absent in Ni-MOF-2 which may be covered by the sharp (100) peak around 9°.

The Fourier-transform infrared (FTIR) spectra of Ni-MOFs are shown in Fig. 1D. In Ni-MOF-1, the obvious peaks appearing in the range of 3,000–3,600 cm^{-1} were ascribed to absorbed H$_2$O molecules. Except for water peaks, Ni-MOF-1 and Ni-MOF-2 exhibited similar peaks. The peaks at around 812 and 742 cm^{-1} are assigned to aromatic deformation vibrations of C–H, and the peaks at around 1,571 and 1,374 cm^{-1} were assigned to the symmetric and asymmetric stretching vibrations of the coordinating carboxyl group [27].

X-ray photoelectron spectroscopy (XPS; Fig. 2) was employed to further identify the composition of Ni-MOF-1 and Ni-MOF-2. Since both of them showed the same spectra, only one spectrum was presented. As shown in Fig. 2A, both of them were mainly composed of C, O, and Ni. In detail, Ni-MOF-1 presented a similar C 1s spectrum to that of Ni-MOF-2. It could be further deconvoluted into two separate peaks which were assigned to the C–C/C = C bond (284.5 eV) and the carboxylic carbon (288.1 eV), respectively (Fig. 2B) [28]. For the Ni 2p spectrum (Fig. 2D), there were two main peaks centered at 856.0 (Ni 2p$_{3/2}$) and 873.7 eV (Ni 2p$_{1/2}$) with two satellite peaks of Ni 2p$_{3/2}$ (around 861.5 eV) and Ni 2p$_{1/2}$ (around 879.8 eV), indicating the existence of Ni^{2+} [29].

The specific surface area and porosity played an important role in electrochemical sensors. As shown in Fig. 3, both the adsorption–desorption isotherm curves had a type IV hysteresis loop, which was a characteristic of mesoporous materials. The specific surface area and pore size of Ni-MOF-1 were 22.26 m^2/g and 22.28 nm, respectively, while 14.40 m^2/g and 23.91 nm for Ni-MOF-2.

2.2. Electrochemical performance of Ni-MOFs

In 0.1 M phosphate buffer solution (PBS) buffer containing 100 μM MNZ, the differential pulse voltammetry (DPV) curves (Fig. 4A) of bare glassy carbon electrode (GCE) presented two irreversible reduction peaks at –0.713 and –0.310 V. However, in a blank PBS buffer, only a weak reduction peak at –0.310 V was observed. Based on this phenomenon, it was reasonable to look at the peak located at –0.310 V as the background current in MNZ detection.
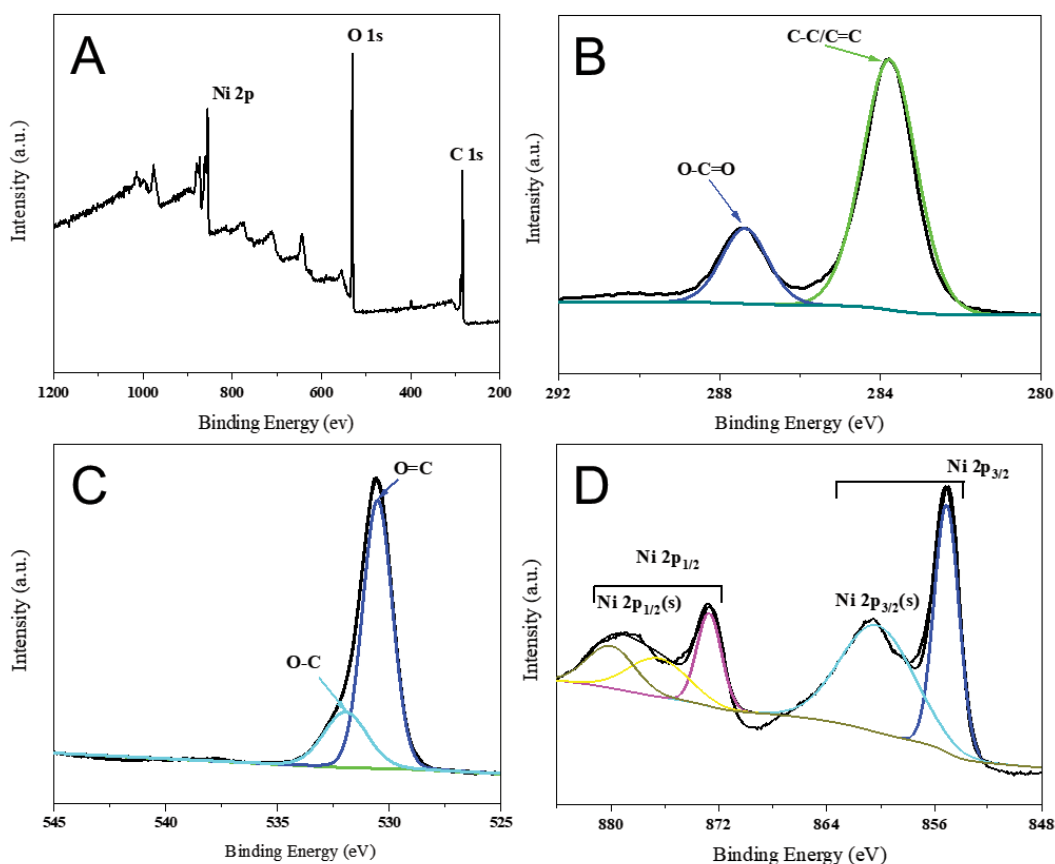

Fig. 2. (A) X-ray photoelectron spectroscopy survey spectrum of Ni-MOF-1 with the high-resolution spectra of (B) C 1s, (C) O 1s, and (D) Ni 2p.
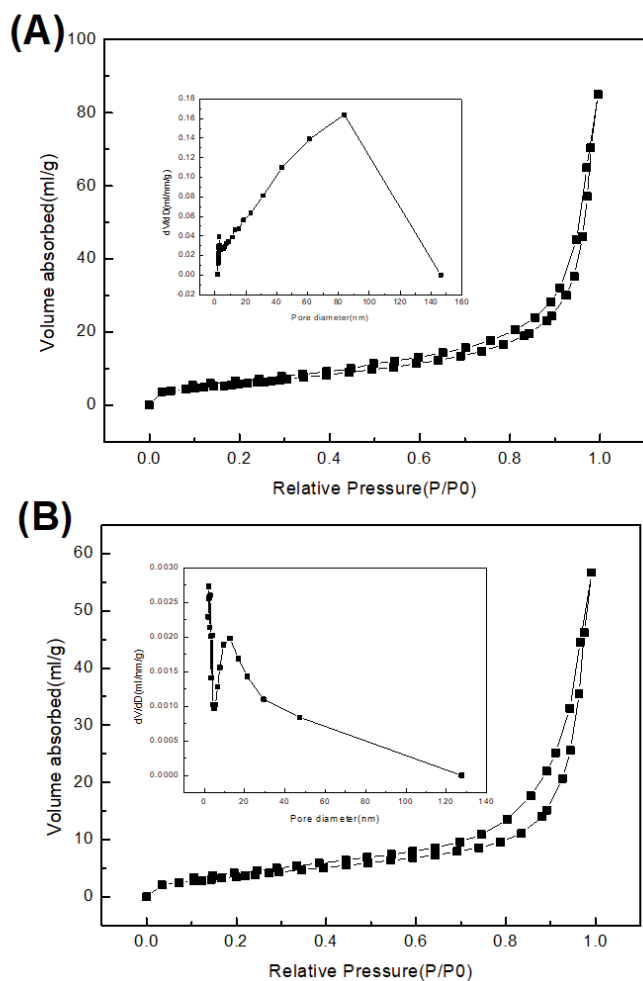
Fig. 3. N$_2$ adsorption–desorption isotherm and pore diameter distribution curves of (A) Ni-MOF-1 and (B) Ni-MOF-2.

According to the literature [30], in an alkaline solution, the dissolved oxygen undergoes a direct four-electron reduction pathway at negative 0.401 V. Since the peak location and intensity varied with the electrode detection environment, the peak at –0.310 V might be attributed to the reduction of dissolved oxygen. For the peak at –0.713 V, it was ascribed to the reduction of the nitro group. Its intensity and potential were significantly different for various electrodes. In cyclic voltammetry (CV) curves (Fig. 4B), when using Ni-MOF-1/CNTs/GCE as the working electrode, the response intensity was much higher than those of the other three electrodes. Its current response reached as high as –169.1 μA at –0.631 V. This phenomenon indicated that Ni-MOF-1/CNTs/GCE showed a higher sensitivity for MNZ [31]. The possible reasons were mainly as follows: (1) the abundant hydroxyl groups in carbon nanotubes (CNTs) and carboxyl groups in MOF could interact with the nitro and hydroxyl groups in MNZ by hydrogen bonds, making MNZ more easily enriched on the surface of the electrode, alleviating the concentration polarization of the electrode and in turn enhancing response intensity. (2) The higher specific surface area of Ni-MOF-1 over Ni-MOF-2 along with its nanosheet stacking, could provide more electrochemical reaction sites

and possibly adsorb more analytes [32]. (3) The introduction of CNTs improved the electron conductivity of the electrode, promoting the electron transfer within the electrode. (4) Ni might help to catalyze the electrochemical reaction. In addition, its higher crystallinity and frame structure might facilitate the charge and ion transfer. Electrochemical impedance spectroscopy (EIS) further offered relative evidence.

As shown in Fig. 4C, the diameter of the semicircle of Ni-MOF-1/CNTs/GCE in the high-frequency range was smaller than that of Ni-MOF-2/CNTs/GCE, indicating the low charge-transfer resistance. Meanwhile, the straight line part at lower frequencies for Ni-MOF-1/CNTs/GCE showed a larger slope than that of Ni-MOF-2/CNTs/GCE, suggesting that the Ni-MOF-1/CNTs/GCE had lower reaction and diffusion resistance. Thus, the electrode modified by Ni-MOF-1 might be more suitable for MNZ detection.

Further investigation was carried out with Ni-MOF-1/CNTs/GCE. Since suitable electrolyte was of great importance to the electrochemical determination [33], the pH effect of electrolyte on the electrochemical reduction responses was studied in 400 μM MNZ here. As can be seen in Fig. 5A and B, the peak current I_p increased with the increase of pH from 8.0 to 12.0, while further increasing pH from 12.0 to 13.0 resulted in a decrease of I_p (Fig. 5B). The reason why pH 13 was an exception might be that strong alkaline environment would induce the electrochemical reaction to run through a kinetic-controlled process instead of a diffusion-controlled process [34]. Therefore, the optimum pH of the PBS buffer used for MNZ detection was set at 12.0 in the following experiments. In addition, E_p dropped linearly with the increase of pH in the range of 8.0 to 12.0 (Fig. 5C), and the linear relationship between E_p and pH could be expressed as Eq. (1).

$$E_p(V) = -0.5406 - 0.0155\text{pH} \tag{1}$$

The CVs of Ni-MOF-1/CNTs/GCE were also recorded at various scan rates from 10 to 200 mV/s in 0.1 M PBS buffer containing 400 μM MNZ (pH 12.0). As shown in Fig. 6A, when increasing the scan rate from 10 to 200 mV/s, the reduction peak current increased and the peak potential shifted negatively (Fig. 6A). The relationship between I_p and the square root of ν (Fig. 6B), could be expressed with a linear equation as Eq. (2).

$$I_p(\mu A) = -12.08129 + 15.33765\nu^{1/2}\left(\text{mV s}^{-1}\right) \tag{2}$$

This result indicated that the electrochemical reaction of MNZ here was based on a diffusion-controlled process. In addition, the negatively shift peak potential proved the electrochemical reaction irreversible [35]. In order to further study its reaction kinetics, the peak potential (E_p) was plotted as a function of the logarithm of scan rate ν. As shown in Fig. 6C, a straight line [Eq. (3)] could describe their relationship.

$$E_p(V) = -0.5639 - 0.03172\ln\nu\left(\text{mV s}^{-1}\right) \tag{3}$$

The electron transfer coefficient α could be calculated from the following formula [Eq. (4)] [36]:
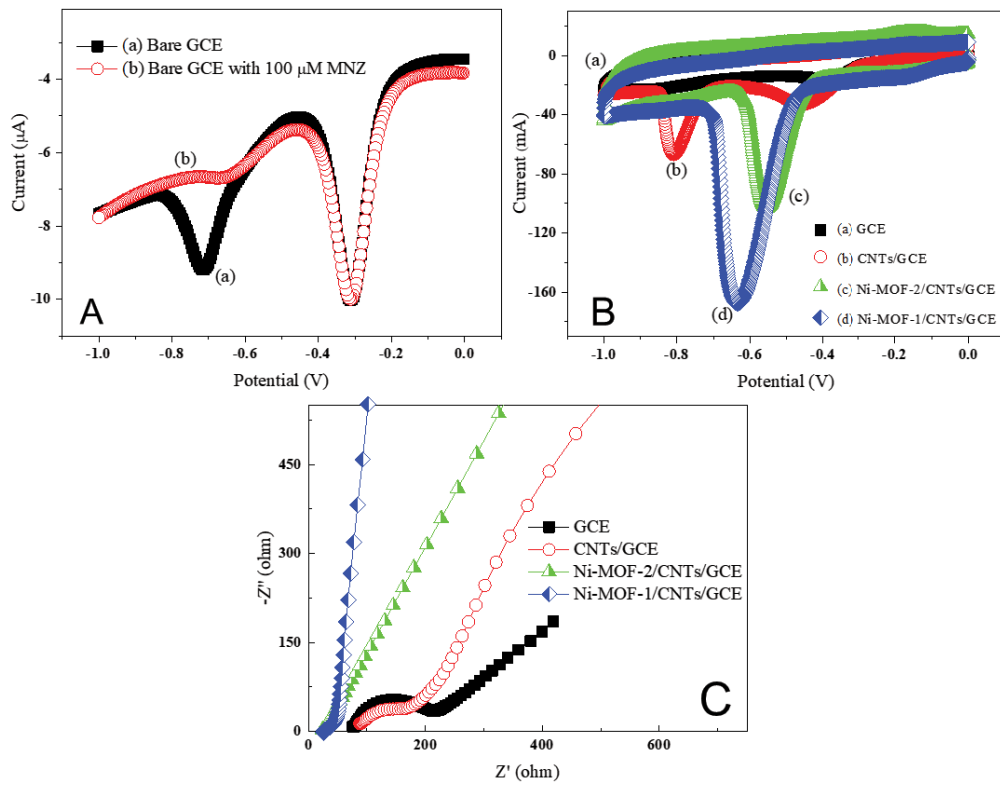
Fig. 4. (A) CV characterization of bare GCE in 0.1 M PBS buffer or 0.1 M PBS buffer containing 100 μM MNZ (pH = 12.0), (B) CV in 0.1 M PBS buffer containing 400 μM MNZ (pH = 12.0), and (C) EIS of different electrodes.
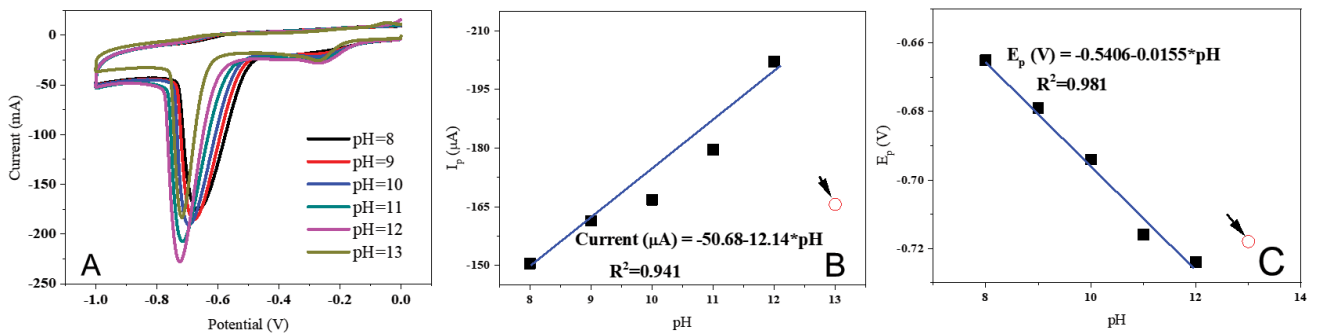

Fig. 5. (A) CVs of Ni-MOF-1/CNTs/GCE in 400 μM MNZ at different pH (100 mV/s), (B) I_p vs pH, and (C) E_p vs. pH.
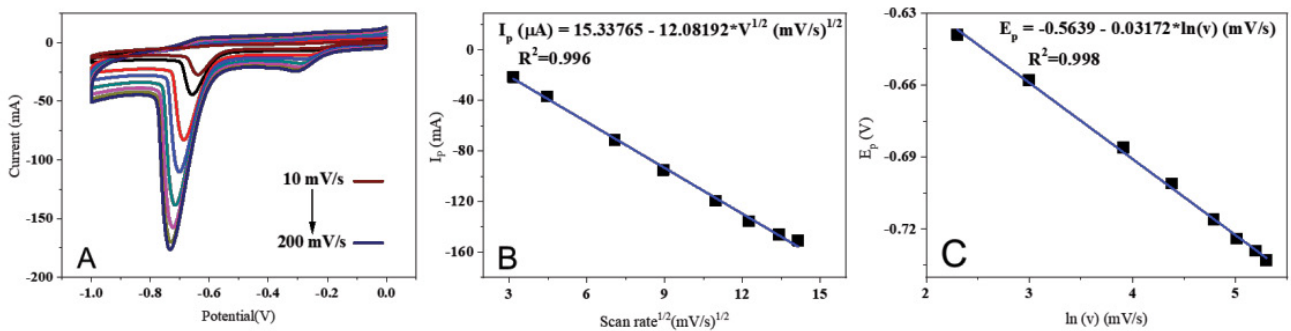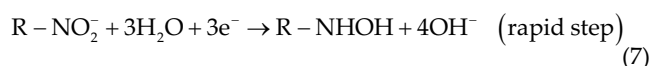

Fig. 6. (A) CVs of Ni-MOF-1/CNTs/GCE in 0.1 M PBS buffer containing 400 μM MNZ (pH 12.0) at different scan rates (from 10 to 200 mV/s), (B) I_p vs. $v^{1/2}$, and (C) E_p vs. ln$v$.

$$\frac{1.15RT}{\alpha F} = 2.303 \times \text{slope} \tag{4}$$

where R, T, and F represented the gas constant (8.314 J/mol·K), room temperature (298 K), and Faraday's constant (9.65×10^4 C/mol), respectively. The slope was directly obtained from Fig. 6C. Therefore, the absolute value of α was calculated to be 0.404. E_p could be expressed with the following equation [37]:

$$E_p = E^0 - \frac{RT}{\alpha n_a F}\left[0.78 + \ln\left(\frac{D_{Ox}^{1/2}}{k^0}\right) + \ln\left(\frac{\alpha n_a F}{RT}\right)^{1/2}\right] - \frac{RT}{2\alpha n_a F}\ln v \tag{5}$$

where E_p was the peak potential (v vs. SCE), and E^0 was the standard potential (v vs. SCE). According to Eq. (5), the electron transfer number n_a was calculated to be 1.002 (approximately equal to 1), indicating that one electron was involved. This result agreed well with the reference. In general, when the rate-determining electron transfer was categorized into a one-electron process ($n_a = 1$), α usually varied between 0.3 and 0.7 [38]. As for the following process in an alkaline medium, it might follow the recommended three-electron transfer mechanism to give hydroxyl amine as suggested in the references [38,39]. Based on the calculated n_a and the references, the following reducing reactions for MNZ in an alkaline solution were proposed as Eqs. (6) and (7).

$$R-NO_2 + e^- \rightarrow R-NO_2^- \ \left(\text{slow step}\right) \tag{6}$$

$$R-NO_2^- + 3H_2O + 3e^- \rightarrow R-NHOH + 4OH^- \ \left(\text{rapid step}\right) \tag{7}$$

Aiming to quantitatively determine the concentration of MNZ, the electrochemical response of Ni-MOF-1/CNTs/GCE to different concentrations of MNZ was investigated by DPV under optimal conditions. In Fig. 7A and B, I_p linearly increased with the increase of MNZ concentration (C). The linear relationship could be expressed as Eq. (8).

$$I_p\left(\mu A\right) = -3.53789 - 0.35825C\left(\mu M\right) \tag{8}$$

From Eq. (8), the slope of the first calibration curve (S) was read as 0.35825, and the standard deviation of the blank current (σ) was 0.003. Thus, the limit of detection (LOD) could be calculated to be 25 nM (confidence level = 95%) according to Eq. (9) [40].

$$LOD = \frac{3\sigma}{S}\left(\frac{S}{N} = 3, n = 10\right) \tag{9}$$

As listed in Table 1, Ni-MOF-1/CNTs/GCE-based electrode of this work outperformed many reported sensors considering its wide linear range and ultra-low LOD, suggesting that Ni-MOF-1/CNTs/GCE was promising for the accurate detection of MNZ. This should be attributed to the sub-micron-assemblies of layered flakes and abundant carboxyl groups of Ni-MOF-1.

Anti-interference ability, stability, and repeatability of the sensor were very important for a sensor's practical application. In this case, in the presence of 200 μM MNZ, some structural analog of MNZ such as tinidazole (TNZ, 3 mM), p-nitrophenol (3 mM), and 2-methylimidazole (Gc, 3 mM) were individually used as interference chemicals. In addition, other substances, which might coexist with MNZ in biological samples, involving glucose (Glc), urea, ascorbic acid (AA, 3 mM), K^+ (20 mM), Na^+ (20 mM), SO_4^{2-} (20 mM) and NO_3^- (20 mM), were investigated separately as interferences too. As shown in Fig. 8, a negligible influence was observed for all the possible coexisting substances. Although nitro-containing structural analogs affected the current response signal, the I_p change of less than 5% could be ignored too, especially considering the much higher concentration of the interfering substances. Thus, Ni-MOF-1/CNTs/GCE displayed excellent anti-interference performance.

To test its reproducibility, six Ni-MOF-1/CNTs/GCE working electrodes were prepared, and the same MNZ solution (400 μM) was detected three times in parallel with the above different working electrodes. A relative standard deviation (RSD) as low as 3.6% was obtained, suggesting
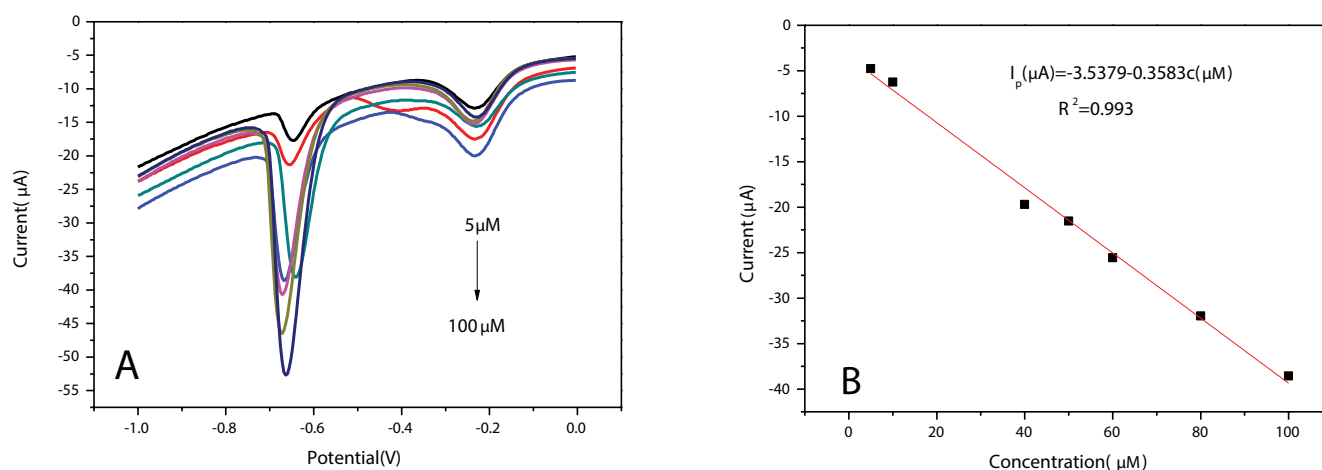

Fig. 7. (A) DPV under different MNZ concentrations based on Ni-MOF-1/CNTs/GCE electrode and (B) I_p vs. MNZ concentration.

Table 1
Comparison of this work with other methods for MNZ detection

Sensors	Methods	Linear range (μM)	LOD (nM)	References
Gr-IL/GCE	DPV	0.1–25.0	47	[41]
SWCNTs/GCE	CV	0.1–200	63	[42]
AgNPs/SF-GR/GCE	DPSV	0.1–20.0	50	[43]
PTH/GCE	DPV	35–500	960	[44]
P-AuE	LSV	0.5–10.0	150	[9]
Ni/Fe-layered double hydroxides/GCE	CV	5–1,595	58	[45]
CPE a-CD	DPV	0.5–103	280	[15]
Ni-MOF-1/CNTs/GCE	DPV	5–100	25	This work
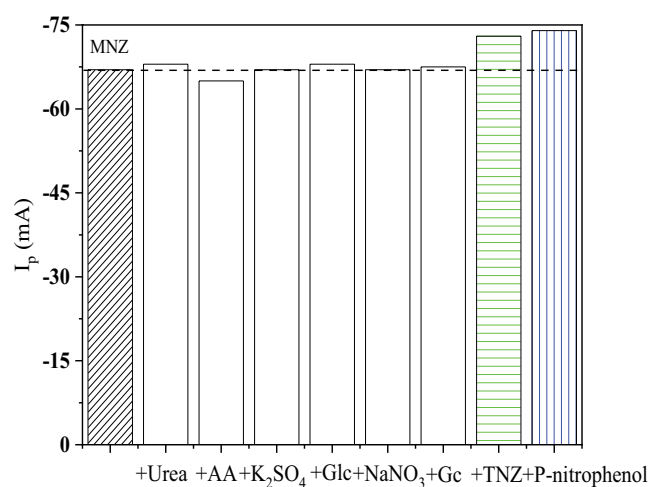
Fig. 8. The anti-interfering performance of Ni-MOF-1/CNTs/GCE in MNZ detection.

Table 2
Recovery tests of MNZ determination

Added (μM)	Found (μM)	Recovery (%)	RSD (%)
25	24.6	98.4	2.2
50	49.3	98.6	2.8
100	97.0	97	2.6

Results were the average of three measurements, $n = 3$.

of Ni-MOF-1/CNTs/GCE was also studied. In contrast to its first detection, an I_p loss below 5% was achieved after placing Ni-MOF-1/CNTs/GCE in a refrigerator (4°C) for two weeks, demonstrating its acceptable stability. Based on the above detection results, Ni-MOF-1/CNTs/GCE could be expected to be used for the quantitative analysis of MNZ in practical samples.

Next, the utility of Ni-MOF-1/CNTs/GCE was investigated by performing the recovery tests according to the standard addition method [25], where MNZ tablets were employed as the standard additive. Three measurements were carried out for every sample under the same conditions except for the difference in MNZ's concentration. Table 2 shows that the electrochemical method using Ni-MOF-1/CNTs/GCE as the electrode was endowed with good MNZ recovery rates (97.0%~98.6%) and considerably narrow RSD (2.2%~2.8%) within the studied dosages, suggesting that the Ni-MOF-1/CNTs/GCE-based electrochemical sensor could serve as a sensitive detection platform of MNZ in practical samples.
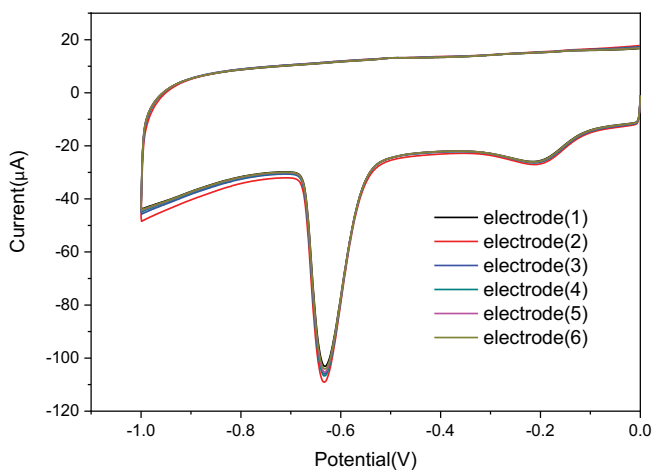

Fig. 9. The repeatability CV curves of Ni-MOF-1/CNTs/GCE in 0.1 M PBS buffer containing 400 μM MNZ (pH 12.0) at 100 mV/s.

its high reproducibility. Besides, after using the same electrode to repeatedly measure MNZ six times, a low RSD of 4.5% was obtained, confirming its good repeatability (details are illustrated in Fig. 9). In addition, the long-term stability

3. Conclusion

In summary, by replacing pure DMF with mixed DMF/water as the solvent, a specific Ni-MOF with some physiochemical uniqueness such as sub-micron layers, rich carboxyl groups, and mesoporous framework, was prepared with a one-step hydrothermal method. Benefiting from its abundant electrochemical reaction sites, lower charge-transfer resistance, lower reaction, and diffusion resistance, a LOD of MNZ as low as 25 nM was observed based on the Ni-MOF/CNT/GCE electrode, which was comparative to many reported electrochemical platforms of MNZ. In addition, the pH-dependent electrochemical process was based on four electrons reduction of the nitro group of MNZ to hydroxylamine. This study will facilitate the application

of novel-metal-based MOF in the sensitive detection of MNZ in the future.

Symbols

E_p	—	Peak potential
I_p	—	Peak current
v	—	Scanning rate
R	—	Gas constant, 8.314 J/mol·K
T	—	Room temperature, 298 K
F	—	Faraday's constant, 9.65×10^4 C/mol
E^0	—	Standard potential (v vs. SCE)
n_a	—	1.002
α	—	0.3–0.7
D_{ox}	—	Diffusion coefficient
k	—	Standard heterogeneous rate constant
σ	—	Standard deviation
S	—	Slope of the calibration curve

Supporting information

The experimental details and some figures (Fig. S1 for the XRD patterns of Ni-MOF-1 and Ni-MOF-2; Fig. S2 for the FTIR spectra of Ni-MOF-1 and Ni-MOF-2) are included in the Supporting information.

Acknowledgements

References

[1] M.S. Refat, H.A. Saad, A.M.A. Adam, Spectral, thermal and kinetic studies of charge-transfer complexes formed between the highly effective antibiotic drug metronidazole and two types of acceptors: σ- and π-acceptors, Spectrochim. Acta A, 141 (2015) 202–210.

[2] C. Ho, D. Sin, K. Wong, H. Tang, Determination of dimetridazole and metronidazole in poultry and porcine tissues by gas chromatography-electron capture negative ionization mass spectrometry, Anal. Chim. Acta, 530 (2005) 23–31.

[3] Y. Vasseghian, E.-N. Dragoi, F. Almomani, Graphene-based materials for metronidazole degradation: a comprehensive review, Chemosphere, 286 (2022) 131727, doi: 10.1016/j.chemosphere.2021.131727.

[4] C. Mahugo-Santana, Z. Sosa-Ferrera, M.E. Torres-Padrón, J.J. Santana-Rodríguez, Analytical methodologies for the determination of nitroimidazole residues in biological and environmental liquid samples: a review, Anal. Chim. Acta, 665 (2010) 113–122.

[5] C.S. Thompson, I.M. Traynor, T.L. Fodey, S.R. Crooks, Improved screening method for the detection of a range of nitroimidazoles in various matrices by optical biosensor, Anal. Chim. Acta, 637 (2009) 259–264.

[6] J. Zhou, J. Shen, X. Xue, J. Zhao, Y. Li, J. Zhang, S. Zhang, Simultaneous determination of nitroimidazole residues in honey samples by high-performance liquid chromatography with ultraviolet detection, J. AOAC Int., 90 (2007) 872–878.

[7] X. Xia, X. Li, S. Ding, S. Zhang, H. Jiang, J. Li, J. Shen, Determination of 5-nitroimidazoles and corresponding hydroxy metabolites in swine kidney by ultra-performance liquid chromatography coupled to electrospray tandem mass spectrometry, Anal. Chim. Acta, 637 (2009) 79–86.

[8] N. Tavakoli, J. Varshosaz, F. Dorkoosh, M.R. Zargarzadeh, Development and validation of a simple HPLC method for simultaneous in vitro determination of amoxicillin and metronidazole at single wavelength, J. Pharm. Biomed., 43 (2007) 325–329.

[9] S. Shi, H. Yu, F. Yang, W. Yao, Y Xie, Simultaneous determination of 14 nitroimidazoles using thin-layer chromatography combined with surface-enhanced Raman spectroscopy (TLC-SERS), Food Biosci., 48 (2022) 101755, doi: 10.1016/j.fbio.2022.101755.

[10] P. Nagaraja, K. Sunitha, R. Vasantha, H. Yathirajan, Spectrophotometric determination of metronidazole and tinidazole in pharmaceutical preparations, J. Pharm. Biomed., 28 (2002) 527–535.

[11] T. Saffaj, M. Charrouf, A. Abourriche, Y. Abboud, A. Bennamara, M. Berrada, Spectrophotometric determination of metronidazole and secnidazole in pharmaceutical preparations, Il Farmaco, 59 (2004) 843–846.

[12] T. Saffaj, M. Charrouf, A. Abourriche, Y. Aboud, A. Bennamara, M. Berrada, Spectrophotometric determination of metronidazole and secnidazole in pharmaceutical preparations based on the formation of dyes, Dyes Pigm., 70 (2006) 259–262.

[13] T. Alizadeh, M.R. Ganjali, M. Zare, P. Norouzi, Selective determination of chloramphenicol at trace level in milk samples by the electrode modified with molecularly imprinted polymer, Food Chem., 130 (2012) 1108–1114.

[14] K. Huang, Q. Jing, Z. Wu, L. Wang, C. Wei, Enhanced sensing of dopamine in the present of ascorbic acid based on graphene/poly (p-aminobenzoic acid) composite film, Colloids Surf., B, 88 (2011) 310–314.

[15] A. Hernández-Jiménez, G. Roa-Morales, H. Reyes-Pérez, P. Balderas-Hernández, C.E. Barrera-Díaz, M. Bernabé-Pineda, Voltammetric determination of metronidazole using a sensor based on electropolymerization of α-cyclodextrin over a carbon paste electrode, Electroanalysis: An Int. J. Devoted Electroanal. Sens. Bioelectron. Dev., 28 (2016) 704–710.

[16] S. Sadeghi, M. Hemmati, A. Garmroodi, Preparation of Ag-nanoparticles/ionic-liquid modified screen-printed electrode and its application in the determination of metronidazole, Electroanalysis: An Int. J. Devoted Electroanal. Sens. Bioelectron. Dev., 25 (2013) 316–322.

[17] J. Huang, X. Shen, R. Wang, Q. Zeng, L Wang, A highly sensitive metronidazole sensor based on a Pt nanospheres/polyfurfural film modified electrode, RSC Adv., 7 (2017) 535–542.

[18] J. Peng, C. Hou, X. Hu, Determination of metronidazole in pharmaceutical dosage forms based on reduction at graphene and ionic liquid composite film modified electrode, Sens. Actuators, B, 169 (2012) 81–87.

[19] M.B. Gholivand, M. Torkashvand, A novel high selective and sensitive metronidazole voltammetric sensor based on a molecularly imprinted polymer-carbon paste electrode, Talanta, 84 (2011) 905–912.

[20] H. Chen, X. Wu, R. Zhao, Z. Zheng, Q. Yuan, Z. Dong, W. Gan, Preparation of reduced graphite oxide loaded with cobalt(II) and nitrogen co-doped carbon polyhedrons from a metal–organic framework (type ZIF-67), and its application to electrochemical determination of metronidazole, Microchim. Acta, 186 (2019) 623, doi: 10.1007/s00604-019-3737-6.

[21] M. Wang, Y. Zhang, S. Bao, Y. Yu, C. Ye, Ni(II)-based metal–organic framework anchored on carbon nanotubes for highly sensitive non-enzymatic hydrogen peroxide sensing, Electrochim. Acta, 190 (2016) 365–370.

[22] Y. Zhou, Z. Mao, W. Wang, Z. Yang, X. Liu, *In-situ* fabrication of graphene oxide hybrid Ni-based metal-organic framework (Ni-MOFs@GO) with ultrahigh capacitance as electrochemical pseudocapacitor materials, ACS Appl. Mater. Interfaces, 8 (2016) 28904–28916.

[23] M. Yue, Y. Jiang, L. Zhang, C. Yu, K. Zou, Z. Li, Solvent-induced cadmium(II) metal-organic frameworks with adjustable guest-evacuated porosity: application in the controllable assembly of MOF-derived porous carbon materials for supercapacitors, Chem. Eur. J., 23 (2017) 15680–15693.

[24] R. Ramachandran, C. Zhao, D. Luo, K. Wang, F. Wang, Morphology-dependent electrochemical properties of

cobalt-based metal organic frameworks for supercapacitor electrode materials, Electrochim. Acta, 267 (2018) 170–180.

[25] J. Yang, P. Xiong, C. Zheng, H. Qiu, M. Wei, Metal–organic frameworks: a new promising class of materials for a high-performance supercapacitor electrode, J. Mater. Chem. A, 2 (2014) 16640–16644.

[26] T.P. Mofokeng, A.K. Ipadeola, Z.N. Tetana, K.I. Ozoemena, Defect-engineered nanostructured Ni/MOF-derived carbons for an efficient aqueous battery-type energy storage device, ACS Omega, 5 (2020) 20461–20472.

[27] G. Zhu, H. Wen, M. Min, W. Wang, L. Yang, L. Wang, X. Shi, X. Cheng, X. Sun, Y. Yao, A self-supported hierarchical Co-MOF as a supercapacitor electrode with ultrahigh areal capacitance and excellent rate performance, Chem. Commun., 54 (2018) 10499–10502.

[28] R. Wang, W. Su, S. Zhang, L. Jin, J. Zhang, H. Bian, Y. Zhang, Application of lignin-derived graphene quantum dots in visible light-driven photoelectrochemical photodetector, Adv. Opt. Mater., (2023) 2202944, doi: 10.1002/adom.202202944.

[29] X. Zhang, N. Qu, S. Yang, Q. Fan, D. Lei, A. Liu, X. Chen, Shape-controlled synthesis of Ni-based metal-organic frameworks with albizia flower-like spheres@nanosheets structure for high performance supercapacitors, J. Colloid Interface Sci., 575 (2020) 347–355.

[30] B. Shapira, E. Avraham, D. Aurbach, Side reactions in capacitive deionization (CDI) processes: the role of oxygen reduction, Electrochim. Acta, 220 (2016) 285–295.

[31] S. Meenakshi, S.J. Sophia, K.J.M. Pandian, High surface graphene nanoflakes as sensitive sensing platform for simultaneous electrochemical detection of metronidazole and chloramphenicol, Mater. Sci. Eng. C, 90 (2018) 407–419.

[32] S. Gao, Y. Sui, F. Wei, J. Qi, Q. Meng, Y. He, Facile synthesis of cuboid Ni-MOF for high-performance supercapacitors, J. Mater. Sci., 53 (2018) 6807–6818.

[33] D. Chen, J. Deng, J. Liang, J. Xie, C. Hu, K. Huang, A core-shell molecularly imprinted polymer grafted onto a magnetic glassy carbon electrode as a selective sensor for the determination of metronidazole, Sens. Actuators, B, 183 (2013) 594–600.

[34] A. Hájková, J. Hraníček, J. Barek, V. Vyskočil, Voltammetric determination of trace amounts of 2-aminofluoren-9-one at a mercury meniscus modified silver solid amalgam electrode, Electroanalysis: An Int. J. Devoted Electroanal. Sens. Bioelectron. Dev., 25 (2013) 295–302.

[35] A. Mao, H. Li, L. Yu, X. Hu, Electrochemical sensor based on multi-walled carbon nanotubes and chitosan-nickel complex for sensitive determination of metronidazole, J. Electroanal. Chem., 799 (2017) 257–262.

[36] P. Dauphin-Ducharme, N. Arroyo-Currás, M. Kurnik, G. Ortega, H. Li, K.W. Plaxco, Simulation-based approach to determining electron transfer rates using square-wave voltammetry, 33 (2017) 4407–4413.

[37] S.E. Kablan, T. Reçber, G. Tezel, S.S. Timur, C. Karabulut, T. Ce. Karabulut, H. Eroğlu, S. Kır, E. Nemutlu, Voltammetric sensor for COVID-19 drug Molnupiravir on modified glassy carbon electrode with electrochemically reduced graphene oxide, J. Electroanal. Chem., 920 (2022) 116579, doi: 10.1016/j.jelechem.2022.116579.

[38] H.B. Ammar, M.B. Brahim, R. Abdelhédi, Y. Samet, Boron-doped diamond sensor for sensitive determination of metronidazole: mechanistic and analytical study by cyclic voltammetry and square wave voltammetry, Mater. Sci. Eng. C, 59 (2016) 604–610.

[39] B. Rezaei, S. Damiri, Fabrication of a nanostructure thin film on the gold electrode using continuous pulsed-potential technique and its application for the electrocatalytic determination of metronidazole, Electrochim. Acta, 55 (2010) 1801–1808.

[40] R. Wang, L. Jiao, X. Zhou, Z. Guo, H. Bian, H. Dai, Highly fluorescent graphene quantum dots from biorefinery waste for tri-channel sensitive detection of Fe^{3+} ions, J. Hazard. Mater., 362 (2016) 315–322.

[41] J. Peng, C. Hou, X. Hu, Determination of metronidazole in pharmaceutical dosage forms based on reduction at graphene and ionic liquid composite film modified electrode, Sens. Actuators, B, 169 (2012) 81–87.

[42] A. Salimi, M. Izadi, R. Hallaj, M. Rashidi, Simultaneous determination of ranitidine and metronidazole at glassy carbon electrode modified with single wall carbon nanotubes, Electroanalysis: An Int. J. Devoted Electroanal. Sens. Bioelectron. Dev., 19 (2007) 1668–1676.

[43] H. Zhai, Z. Liang, Z. Chen, H. Wang, Z. Liu, Z. Su, Q. Zhou, Simultaneous detection of metronidazole and chloramphenicol by differential pulse stripping voltammetry using a silver nanoparticles/sulfonate functionalized graphene modified glassy carbon electrode, Electrochim. Acta, 171 (2015) 105–113.

[44] M.M. Rahman, X.B. Li, Y.D. Jeon, H.J. Lee, S.J. Lee, J.J. Lee, Simultaneous determination of ranitidine and metronidazole at poly(thionine) modified anodized glassy carbon electrode, J. Electrochem. Sci. Technol., 3 (2012) 90–94.

[45] K. Nejati, K. Asadpour-Zeynali, Electrochemical synthesis of nickel-iron layered double hydroxide: application as a novel modified electrode in electrocatalytic reduction of metronidazole, Mater. Sci. Eng. C, 35 (2014) 179–184.

Supporting information

S1. Experimental

S1.1. Preparation of Ni-MOF

Ni(NO$_3$)$_2$·6H$_2$O, terephthalic acid (PTA), metronidazole (MNZ), and N,N-dimethylformamide (DMF) were purchased from Aladdin (Shanghai, China). Other frequently used reagents and solvents were used as supplied without further purification. Nickel-based metal–organic framework (Ni-MOF) was synthesized with hydrothermal method. Typically, 0.5 g Ni(NO$_3$)$_2$·6H$_2$O and 0.5 g PTA were dissolved in a mixture of DMF (25 mL) and distilled water (5 mL). After being stirred for 10 min, the mixing solution was transferred to a Teflon-lined autoclave. Then, the autoclave was placed in an oven and kept at 130°C for 24 h. Later, the autoclave was taken out and naturally cooled to room temperature in the air. The resulting product was washed with DMF for three times to remove the unreacted starting material, and then washed with ethanol for several times. Finally, the obtained precipitate was dried at 60°C for 24 h, and the final product was marked as Ni-MOF-1. For a comparative study, Ni-MOF-2 was prepared in pure DMF. Its preparing process completely followed that of Ni-MOF-1.

S1.2. Characterization

The structure and phase of Ni-MOFs were determined by X-ray powder diffraction using PANalytical Empyrean (Almelo, Netherlands). The morphologies of the samples were observed by means of scanning electron microscopy (ZEISS Sigma 300, Tokyo, Japan). Surface chemistry properties of the samples were obtained from the high-resolution X-ray photoelec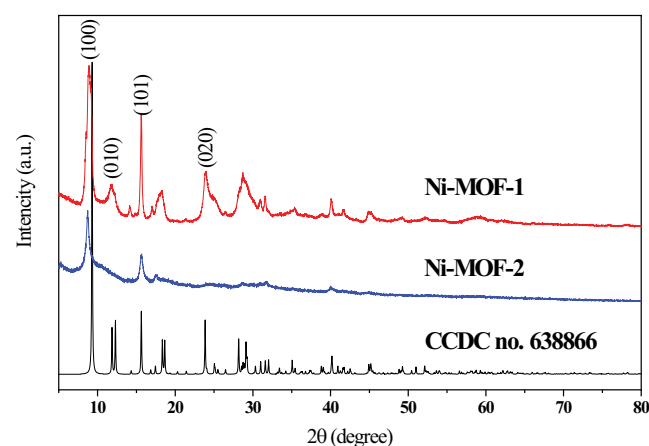tron spectroscopy (Thermo Scientific K-Alpha, Manchester, UK). Fourier-transform infrared spectrometer (Thermo Scientific Nicolet iS50, Austin, USA) was used to determine the functional groups in the materials, The specific surface areas (S_{BET}) were collected on the Brunauer–Emmett–Teller (BET) (BSD-PS(M)).

S1.3. Electrochemical measurement

Electrochemical properties of the MOF materials were investigated with CHI760E electrochemical workstation (Chenhua, Shanghai, China). Electrochemical impedance spectroscopy (EIS) was tested between 0.1–100 kHz. Cyclic voltammetry and differential pulse voltammetry were carried out in 0.1M phosphate buffer solution containing MNZ at room temperature. The working electrode was fabricated as follows. Firstly, 9.0 mg Ni-MOF and 1.0 mg multi-walled carbon nanotubes were ultrasonically dispersed in 10.0 mL isopropanol for 20 min. Then, 10 μL of the mixture was dropped onto the surface of the glassy carbon electrode with a microsyringe. After dried naturally, the electrode was coated with 3 μL 0.1% Nafion solution. In addition, to prepare the wastewater sample, five metronidazole tablets and interfering substance were fully ground separately, then an accurately weighed amount of powder was dissolved in deionized water, ultrasonicated for 10 min, and followed by filtrating the suspension with Büchner Vacuum Funnel. Finally, an appropriate amount of solution was taken and diluted with 0.2 M phosphate buffer solution to obtain the 500 μM MNZ standard solution. Other MNZ concentration solutions were obtained by further diluting the above MNZ standard solution with phosphate buffer solution.

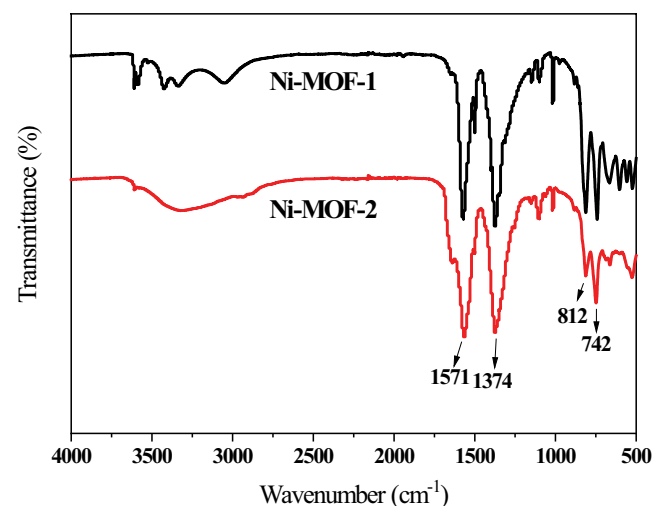Fig. S1. X-ray diffraction patterns of Ni-MOF-1 and Ni-MOF-2.

Fig. S2. Fourier-transform infrared spectra of Ni-MOF-1 and Ni-MOF-2.